*clean technologies*

MDPI

*Article*

# Drying Kinetics of Macroalgae as a Function of Drying Gas Velocity and Material Bulk Density, Including Shrinkage

**Craig Walker and Madoc Sheehan ***

College of Science and Engineering, James Cook University, Townsville 4811, Australia; craig.walker@my.jcu.edu.au
* Correspondence: madoc.sheehan@jcu.edu.au

**Abstract:** Macroalgae have many potential applications and can make important contributions to sustainability and circular economy objectives. Macroalgae are degradable high-moisture biomaterials and drying is a necessary step, but drying is an energy and capital-intensive part of their production process. This study presents convective drying curves for commercially promising fresh and saltwater species (*U. ohnoi* and *O. intermedium)*, obtained over a range of industry-relevant drying gas velocities (0.3–2 m/s) and material bulk densities (33–100 kg/m$^3$). Pragmatic diffusion-based drying models that account for the influence of drying gas velocity, material bulk density, and material shrinkage are presented. Results provide critical insights into the validity of diffusion model assumptions for compressible biomaterials and new mechanisms describing gas penetration into such materials are proposed. The drying models provided in this work demonstrate a high degree of accuracy for both species.

**Keywords:** macroalgae; drying rates; gas penetration; bulk density; shrinkage; modeling



**Citation:** Walker, C.; Sheehan, M. Drying Kinetics of Macroalgae as a Function of Drying Gas Velocity and Material Bulk Density, Including Shrinkage. *Clean Technol.* **2022**, *4*, 669–689. https://doi.org/10.3390/cleantechnol4030041

Academic Editor: Patricia Luis

Received: 21 June 2022
Accepted: 19 July 2022
Published: 22 July 2022



## 1. Introduction

The grand challenges of climate change and sustainability have led to a growing focus on the production and use of renewable materials, such as macro and microalgae. As photosynthetic organisms that sequester $CO_2$ during growth, algae can help society transition away from fossil fuels and assist in achieving emission reduction goals (Paris Agreement 2015 [1]). Furthermore, algae are a renewable biomaterial that can be used to produce a range of products, including fertilizers and animal feeds, human food supplements, nutraceuticals, specialty chemicals, and bioenergy [2,3]. Algae have also been demonstrated to assist in bioremediation applications as diverse as mine-tailings water treatment [4,5] and aquaculture wastewater treatment [6,7]. Such examples demonstrate the potential to use algae to develop circular economy solutions within existing production systems.

Macroalgae are a plant-like organism that can grow in either fresh or saltwater, depending on species. Growth rates of macroalgae are very high and saltwater species such as *Ulva ohnoi* (Chlorophyta) can achieve substantial growth rates [7]. Other species, such as the freshwater macroalgae *Oedogonium intermedium* (Chlorophyta), show promise in energy production applications [8] and as a supplement to reduce cattle greenhouse gas emissions [9,10]. Such examples demonstrate potential for such algae species to be useful products of industrial processes.

There has been comparatively little attention to the optimization of macroalgae production processes. Raw algae products are typically of low value, and optimization of all processing steps is required for economic viability. The high water content of the centrifuged or filtered macroalgae (80–90%$_{WB}$) is an issue for many of the potential production pathways. For example, high moisture content can cause substantial problems in biodiesel production [2], and conventional pyrolysis of algae for the production of biogas or biochar requires very low moisture (0–15%) for efficient processing [11]. The very high ratio of moisture to dry mass also incentivizes drying to reduce weight and volume for transportation

to markets and/or additional processing. Furthermore, the removal of moisture increases the storage life of algal products through the inhibition of spoilage due to unwanted microbial growth. However, drying is an energy-intensive process, potentially responsible for the single highest energy cost in an algae production process [12]. Optimization and careful design of drying equipment are therefore priorities for cost-effective development of macroalgae bioresources.

Convective dryers are widely used in biomass drying applications and provide significantly enhanced drying rates compared with other dryer types. In a convective dryer, the drying process for materials with internally bound moisture, such as macroalgae, involves three simultaneous stages: heat transfer to the material (usually via convective transfer); mass transfer of moisture (typically diffusion) to the exposed material surfaces; and convective mass transfer of moisture to the surroundings [13]. The mass transfer through the material is partially driven by a moisture concentration gradient between the material and the surroundings. This leads to a rate of drying that typically reduces over time (i.e., the falling rate) as the concentration of moisture throughout the algae material decreases [14], and such drying is referred to as diffusion-controlled drying. The drying rate, typically obtained through experimentation, is an important characteristic of a material as it directly enables the determination of dryer residence times and equipment sizing. Modeling such rates can also be useful to understanding the fundamental processes that are occurring. Key dryer design variables that can potentially affect the drying rate include drying gas temperatures and gas flow rates (i.e., the gas velocity). However, it is also important to understand the impact of other material characteristics that influence biomaterial drying rates, such as the compressible nature of algae (represented by bulk density) as well as material shrinkage (represented by a material's characteristic length).

While there is some evidence to suggest that macroalgae shrink during the drying process [15], there have been relatively few studies of macroalgae drying reported in the literature. Vega-Galvez et al., 2008 [16] modeled drying of the brown macroalgae *Macrocystis pyrifera*, Gupta et al., 2011 [17] studied drying of the macroalgae *Himanthalia enlongata*, Uribe et al., 2017 [18] studied the drying kinetics for the brown macroalgae *Durvillaea antarctica*, and Lemus et al., 2008 [19] and Tello-Ireland et al., 2011 [20] investigated drying of the red macroalgae *Gracilaria chilensis*. In all these examples, the impact of temperature on the diffusion coefficient and drying rate was examined (in the range 40 to 80 °C), while the gas velocity remained constant, with a value chosen in the range 1.5–2 m/s. Recent work by Walker et al., 2020 [14], which we build on in this paper, looked at the drying of *U. ohnoi* and *O. intermedium* for a range of temperatures, but also under constant gas velocity conditions. In a purely diffusion-controlled drying process where surface convection is not rate limiting, the impact of gas velocity on drying rates would be expected to be negligible. For example, when Mohamed et al., 2007 [21] investigated the thin layer drying kinetics of the macroalga *Gelidium sesquipedale* at very low gas velocities (0.04 to 0.15 m/s), they found purely falling rate drying (i.e., diffusion-controlled) and a minimal influence of gas velocity. However, when Djaeni and Sari., 2015 [22] undertook convective drying of the macroalga *Eucheuma cottonii* at much higher gas velocities of 5 m/s and 7 m/s, results showed an increase in drying rate with increasing gas velocity. Similar observations of the influence of gas velocity on drying rates in diffusion-controlled systems have also been made for biomaterials that have similar compressible and porous characteristics to macroalgae. This includes Chkir et al., 2015 [23] in their work on drying brewers' grain and research undertaken by Bezzina et al., 2018 [24] on drying sugar cane bagasse fiber. Both these studies found that drying rates increased with increasing gas velocity, despite being entirely falling-rate or diffusion-controlled processes.

In Bezzina et al.'s, 2018 [24] study of bagasse fiber, bulk density was also found to have a significant influence on the drying rate. However, studies of the influence of bulk density on drying of compressible materials are extremely rare in the literature and our understanding of the mechanisms that occur in these types of biomaterials is very limited. Some studies report relationships between effective diffusivity and a material's porosity

and tortuosity (see, for example, [25,26]). However, utilizing such relations requires a priori knowledge of both porosity and tortuosity, with the latter being very challenging to define for a heterogenous and tangled fiber such as macroalgae. Use of such relations is further complicated by materials that exhibit shrinkage, such as macroalgae, for which applicable relations are not well-developed. A more practical and measurable material property is bulk density, which can be more useful when developing models for industrial applications such as dryer control and dryer design.

This study investigated the influence of gas velocity, density, and shrinkage for two different species of macroalgae (*U. ohnoi* and *O. intermedium*). Pragmatic drying rate models based on Fick's Second Law were developed for a range of initial material bulk densities and typical industrial drying air velocities, with inclusion of the effects of material shrinkage. Models of the effects of these variables on drying rate parameters, such as the effective diffusivity, are provided. The aim of the modeling is to provide an accurate representation of the drying rate for the target species. The model is intended to be sufficiently pragmatic that it can utilized by industry to predict dryer performance or optimize dryer design. Furthermore, the modeling also seeks to provide insights into the underlying mechanisms involved in drying porous biomaterials. Based on the observed effects of density and gas velocity, an analysis of the validity of model assumptions for compressible biomaterials is provided, and a mechanism describing the effect of gas velocity on drying rates is proposed.

## 2. Experiments

### *2.1. Materials*

The saltwater species *U. ohnoi* and freshwater species *O. intermedium* were both obtained fresh from the Aquaculture Research Facilities Unit (MARFU) at James Cook University in Townsville, Australia. *U. ohnoi* forms two-cell-thick rectangular sheets that are approximately 10 cm wide, and *O. intermedium* forms long strings one-cell-thick, which have a tendency to clump. Visual images of these macroalgae immediately following dewatering are shown in Figure 1. The porous and compressible nature of the biomaterials is noticeable in these images and the bulk density of the macroalgae ranges from 30 to 50 kg/m$^3$ loose, up to 500 kg/m$^3$ or higher when compressed with significant force.

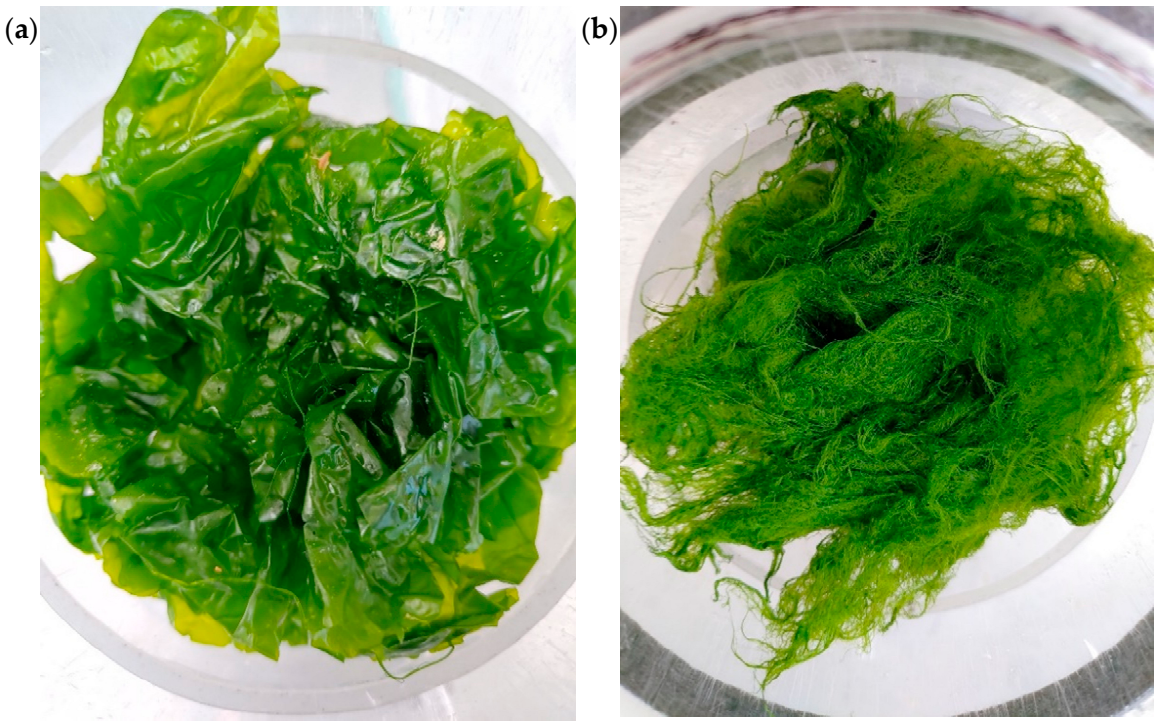


**Figure 1.** Fresh dewatered algae samples: (**a**) *U. ohnoi;* (**b**) *O. intermedium*.

Prior to drying tests, all surface moisture was removed from the algae samples with a lab-scale centrifuge (Koh-I-Noor Engineering Works, Punjab, Pakistan) operated at 2800 g. Dry weight measurements were obtained using a Sartorius MA-45 (AG, 37075 Goettingen, Germany) operated at 110 °C. Across all tests undertaken, the initial moisture content (and 95% confidence interval) for *U. onhoi* was 81.73% dry basis (1.4%) and for *O. intermedium* was 83.54% dry basis (1.1%). Equilibrium moisture contents for both species were determined in previous work by the Authors [14].

### 2.2. Apparatus

Figure 2 shows the overall system diagram of the drying apparatus utilized for this research. For each run, fresh dewatered samples were placed in the sample container and the change in sample mass was recorded in situ over time, under controlled temperature and gas flow rate conditions. A load cell (OMEGA LCAE-1 kg, OMEGA Engineering, CT, USA) and a data logger were used to measure the sample mass in situ. To avoid interference from gas drag on the sample mass, the gas bypass was engaged for ten seconds every three minutes during a drying run. Mass data were averaged over this sampling time to reduce noise in load cell recordings. The sample container was made of clear acrylic to allow for in situ image collection and visual analysis of material during drying. A camera mount was attached next to the sample container, where a GoPro camera (Hero 5 Black, GoPro. Inc., San Mateo, CA, USA) was attached to take images of the material as it dried. The sample chamber had a fixed volume, which allowed for control of the material's bulk density. Different initial masses of material were loaded into the chamber, with the material constrained within a prescribed volume between two mesh screens. Typical initial wet sample masses used in the drying tests were in the order of 20 g. The center of mass of the sample container was placed directly below the load cell. Full apparatus design and instrument calibration details can be found elsewhere [27]. The hot air source was ambient air drawn through four hot air guns (PHG 620 DCE, Bosch, Gerlingen, Germany), providing a controllable gas flow rate and temperature. Ports were added to the piping to allow for measurement of gas conditions using an anemometer (AM-4214SD, Lutron Electronics Enterprise, Taipei, Taiwan), a relative humidity probe (Center 313, Center Technology Corp., Taipei, Taiwan), and a k-type thermocouple.

### 2.3. Experimental Design

In earlier work by the Authors, the impact of temperature on drying of the two target algae species was investigated [14]. In that work, equilibrium moisture contents were reported and the Arrhenius pre-exponential factor ($E_a$) was determined. These values were utilized in the modeling reported in this research. In this work, the effects of air velocity and material bulk density on drying rates of the two macroalgae were studied using the custom-built convective drying apparatus operated at 50 °C. Evaluation of the existence of interaction effects was performed using a two-level factorial design [28]. The condition sets used for both macroalgae are summarized in Table 1, with those used in the two-level factorial design listed in italics. All condition sets were repeated in triplicate. The raw experimental data of mass against time from the experiments were converted to dimensionless moisture ratio versus time ($MR = \frac{(M-M_e)}{(M_0-M_e)}$), where $M$ is the sample moisture content, $M_0$ is the initial sample moisture content, and $M_e$ is the equilibrium moisture content. All moisture contents are expressed on a dry basis.

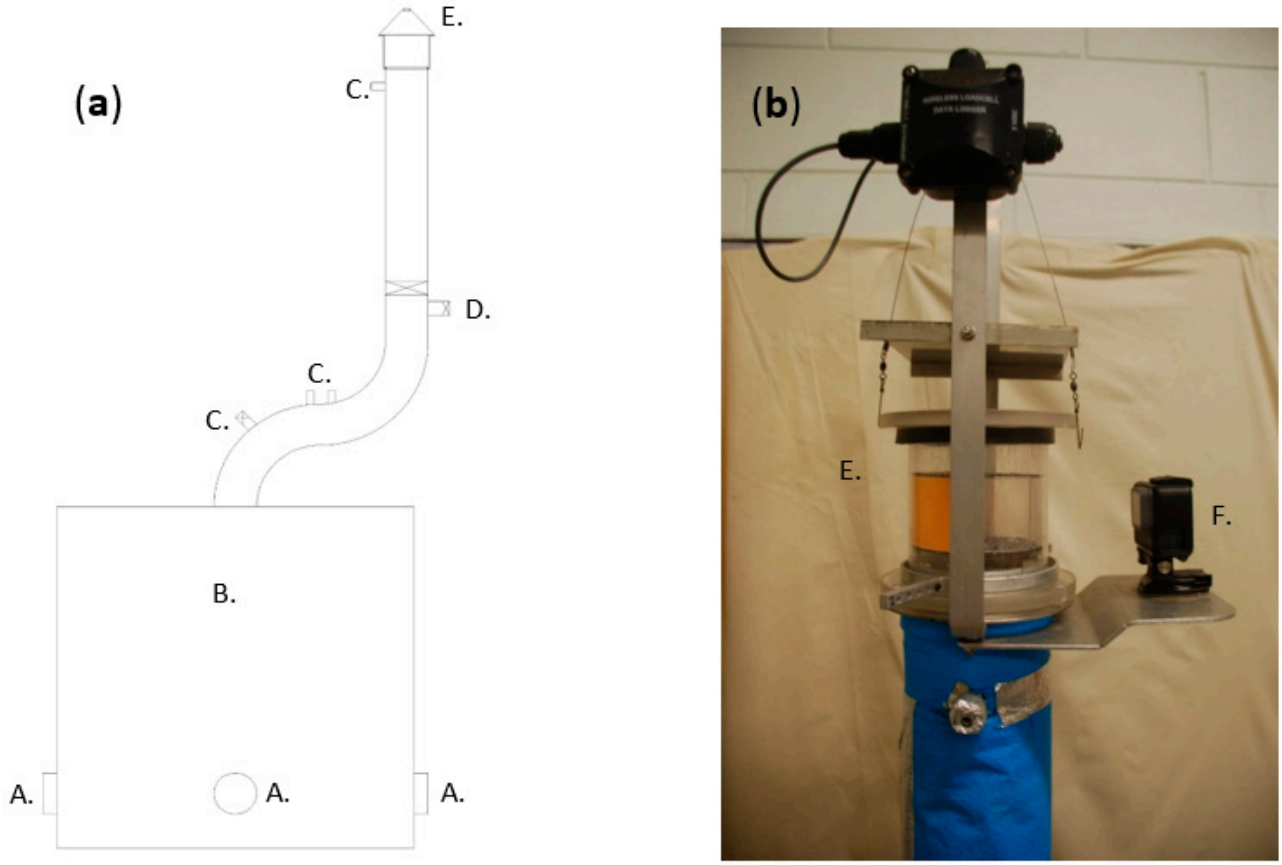


**Figure 2.** (**a**) Schematic of the convective drying system. (**b**) Sample container and load cell setup. Component labels include: A, Heat gun input ports; B, Mixing chamber; C, Instrumentation ports; D, Gas bypass valve; E, Sample container and load cell; F, Camera setup.

**Table 1.** Experimental condition sets used for both macroalgae.

| Gas Velocity $v_g$ (m/s) | Initial Bulk Density $\rho$ (kg/m$^3$) |
|---|---|
| 0.4 | 66 |
| 0.7 | 66 |
| 1.1 | 66 |
| 1.3 | 66 |
| 1.7 | 66 |
| 2.0 | 66 |
| 2.0 | 33 |
| 2.0 | 50 |
| 2.0 | 100 |
| 0.4 | 33 |

## 3. Theory

Modeling of drying for materials with internal moisture is typically performed by taking a mechanistic approach that solves fundamental heat and mass transfer relations using differential equations or via an empirical/semi-empirical approach, using fitted equations and lumped parameters. The mechanistic approach is limited by both a lack of fundamental properties describing macroalgae (such as heat and mass transfer coefficients) as well as the difficulty in solving the resulting partial differential equations, which limit the potential industry uptake. In this work, a more pragmatic semi-empirical approach is

taken that solves Fick's Second Law of Diffusion (F2L) and lumps the effects of material density and gas velocity into a single diffusion coefficient ($D_0$), whilst still accounting for material shrinkage. Such an approach is widely accepted for biomaterial drying and has been previously used to represent drying of many different types of biomaterials, including several other macroalgae species [16,18,19,29,30]. F2L for a one-dimensional semi-infinite slab of material (shown in Figure 3) is given by in the following equation.

$$\frac{\delta C}{\delta t} = D_e \frac{\delta^2 C}{\delta x^2} \tag{1}$$

where $C = f(x,t)$ is the concentration at a given point and time, $x$ is the distance of the point from the boundary surface, $t$ is time, and $D_e$ is the effective diffusion constant. In this model, a number of assumptions are utilized: diffusion represents the overall drying mechanism; there is a uniform initial distribution of moisture throughout the material; drying is one-directional and moisture vapor travels out of the sheet surface; moisture on the sheet surface is immediately removed via bulk convective mass transfer, ensuring that the surface concentration is constant and at the equilibrium concentration and that diffusion is the rate-limiting step; and the diffusion coefficient is not a function of distance or time. A conceptualization of the model geometry can be seen in Figure 3 and the mathematical expression of the model boundary conditions for the PDE can be found elsewhere [27]. When F2L is solved analytically for the moisture ratio ($MR$) for a slab geometry of thickness $x = L$, the following series solution is obtained:

$$MR = \frac{8}{\pi^2} \sum_{n=0}^{\infty} \frac{1}{(2n+1)^2} \exp\left(\frac{-(2n+1)^2 \pi^2 D_e t}{4L^2}\right) \tag{2}$$

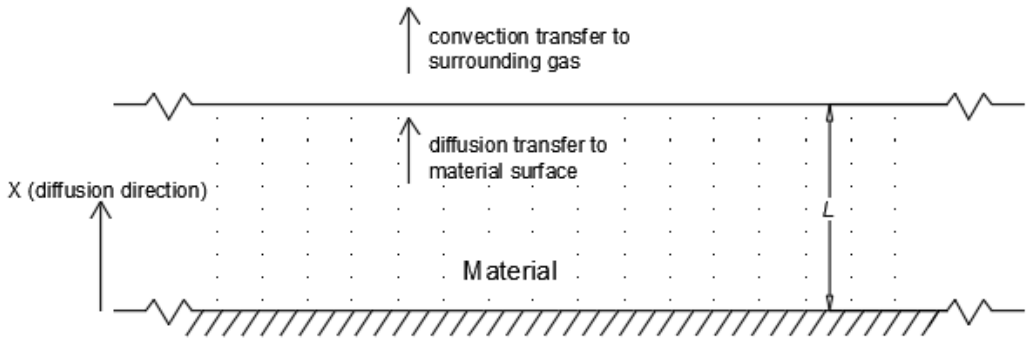


**Figure 3.** Diagram of the material geometry assumed in the development of the Fick's law analytical drying model.

The parameter $D_e$ is a lumped parameter that represents the effective diffusivity of the material and is therefore some function of all variables affecting the drying rate. The $D_e$ parameter is used as the manipulated variable in parameter estimations and optimized values for $D_e$ for each experimental data set are calculated. However, the impact of temperature is often described using an Arrhenius expression for $D_e$ (Equation (3)), whereby $D_0$ is the lumped parameter used to describe the effects of other variables on the drying rate. A strong Arrhenius relationship between effective diffusivity and temperature has been demonstrated in previous radiative drying research for both species of algae (*U. ohnoi* and *O. intermedium*) [14].

$$D_e = D_0 \exp\left(-\frac{E_a}{RT}\right) \tag{3}$$

The analytical solution to Fick's Second Law was fit to experimentally derived moisture ratio versus time data sets. Model fitting was performed by minimization of the total sum of square errors between the model and experimental data (summarized in Equation (4)) for each data set, with the model representing the best fit to all three sets of data at a

given condition. Ten terms of the infinite series ($n$ = 10 in Equation (2)) were used in modeling to ensure convergence in the infinite series solution [31]. These calculations were performed using Microsoft Excel using the solver function with the GRG nonlinear solver method assuming constant relative variance in the experimental data. The objective function is summarized in Equation (4), where $m$ corresponds to the number of data sets. The objective function ($Obj$) was minimized by varying the magnitude of the effective diffusivity parameter ($D_e$).

$$Obj = \sum_{m=1}^{3} \left( \sum \left( MR_{model} - MR_{exptl} \right)^2 \right) \tag{4}$$

*Modeling Shrinkage*

Image capture and shrinkage image analysis were performed in triplicate for both algae species. For *U. ohnoi*, the drying conditions analyzed were 50 °C, 0.7 m/s air velocity, and 66 kg/m$^3$ bulk density, while for *O. intermedium* the conditions were 50 °C, 2.0 m/s air velocity, and 66 kg/m$^3$ bulk density. These images were used to determine the change in the slab width (i.e., $L$) during drying for both species. Slab widths were converted to a non-dimensional property via: $L_D = \frac{L_t - L_\infty}{L_0 - L_\infty}$, where $L_t$ is the slab width at time $t$, $L_0$ is the initial slab width, and $L_\infty$ is the final slab width (at $t = \infty$). The difference between the initial and final slab width is given by $L_\Delta$. The properties of $L_0$ and $L_\infty$ are straightforward values to determine experimentally. The value $L_D$ represents the fraction of volume losses that are yet to occur during drying. For example, at $t = 0$, $L_D$ is equal to 1 and indicates that no volume loss has occurred; at $t = \infty$, $L_D$ is equal to zero and indicates that all volume losses from drying have occurred. This makes both the moisture content and slab width non-dimensional values with the same range, facilitating comparison of moisture and volume losses over time. Examples of $L_D$ vs. $MR$ are shown in Figure 4 for the raw data sets. Correlation of $L_D$ and $MR$ obtained from the experimental data was performed in SPSS and statistical analysis demonstrated $MR$ and $L_D$ to be linearly correlated with statistical significance at the 95% confidence level across all data sets.

To include the impacts of volume loss in the F2L drying rate model described in Equation (2), $L_D$ was equated to $MR$ (Equation (5)). The slab width at any time $t$ ($L_t$) was related to the $MR$ value at the same time ($MR_t$) via Equations (6) and (7) rather than from direct measurement of length versus time.

$$L_D = MR = \frac{L_t - L_\infty}{L_0 - L_\infty} \tag{5}$$

$$L_t = L_\infty + MR_t(L_\Delta) \tag{6}$$

$$L_\Delta = L_0 - L_\infty \tag{7}$$

For convenience and in the interests of developing a pragmatic model to predict $MR$ versus time profiles, the predicted $MR$ utilizes the previous time-step's $L$. In essence, it assumes that each new length represents the slab's dimensions up to that point. Although not formally correct, this approach avoids having to solve the full PDE system described in Equation (1), but with varying boundary conditions. The method calculates $MR$ at time $t$ through approximating drying of a slab of width $L_t$ from $t$ = 0 to $t = t$, but given a sufficiently small time-step (one-minute steps were used in this study) this approximation works well and is simple to implement. Thus, by substitution, F2L including shrinkage is as follows (Equation (8)):

$$MR_t = \frac{8}{\pi^2} \sum_{n=0}^{10} \frac{1}{(2n+1)^2} \exp\left( -\frac{(2n+1)^2 \pi^2 D_e t}{4(L_\infty + MR_{t-\Delta t} L_\Delta)^2} \right) \tag{8}$$

Model fitting for the optimized $D_e$ value that best fit the experimental *MR* versus time data was performed with both the constant *L* model (Equation (2)) and the shrinkage model (Equation (8)).

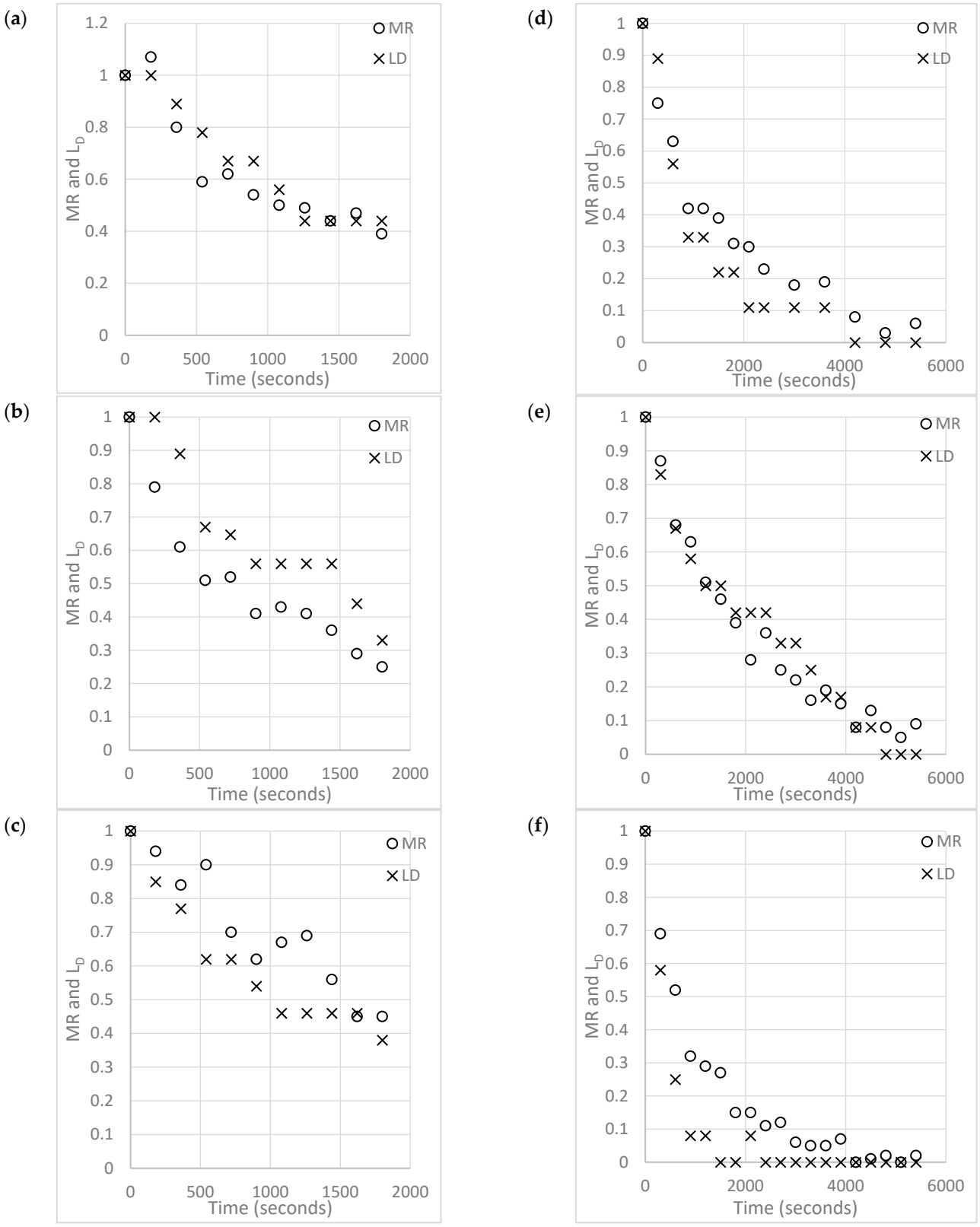


**Figure 4.** Triplicate comparison between *MR* and $L_D$: (**a**–**c**) *U. ohnoi* at 50 °C, 0.7 m/s air velocity, and 66 kg/m$^3$; (**d**–**f**) *O. intermedium* at 50 °C, 2 m/s air velocity, and 66 kg/m$^3$.

## 4. Results

### *4.1. Raw Data and Model Validity*

Figure 5 shows example triplicate *MR* versus time data sets for both species at 50 °C, 66 kg/m$^3$ initial density, and 1.1 m/s airflow. Across all runs, the data repeatability was high. Variance between triplicates was low for *U. ohnoi*, but variance between triplicates was higher for some *O. intermedium* condition sets. *O. intermedium*'s composition of single-cell-wide strands tends to become entangled and to form clumps during harvesting and dewatering, leading to higher variance compared with *U. ohnoi*.

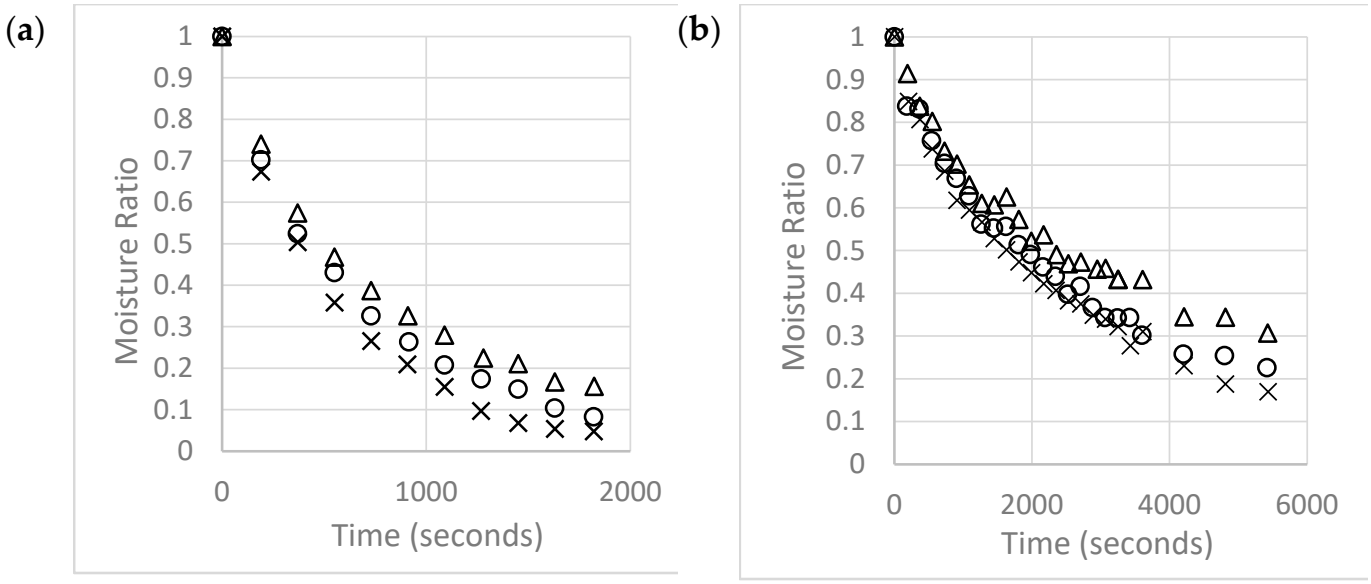


**Figure 5.** Examples of triplicate variance in MR versus time curves for (**a**) *U. ohnoi*; and (**b**) *O. intermedium*.

For the F2L model to be a reasonable representation of the mechanism involved in macroalgae drying, a single falling rate should be observed in the experimental data. A falling rate provides a good indication that drying is limited by diffusive moisture transfer and that F2L is an appropriate mechanistic description. The rate of change of the averaged experimental moisture ratios was obtained using a second-order forward-Taylor-series method. Example graphs of the rate of change of MR against time for the two species are shown in Figures 6 and 7. The figures also include the rate of change of *MR* calculated by deriving the fitted F2L model (Equation (2)) as an example of the expected shape of a single falling rate drying period. A constant rate period during drying would show as a horizontal line.

The experimental data show no indication of a constant rate drying period, and statistical analysis comparing the experimental data and model curve for $dMR/dt$ showed high correlation at the 95% confidence level. This suggests that drying of both macroalgae species under the experimental conditions tested is well-represented by a diffusion-dominated mechanism and F2L.

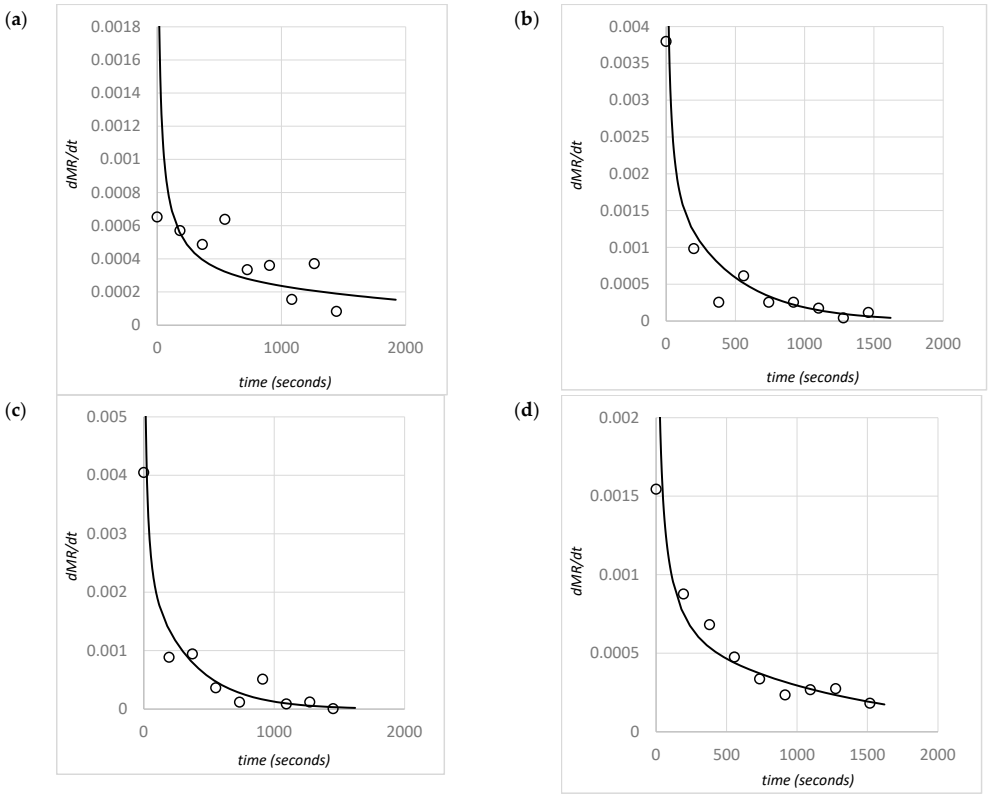


**Figure 6.** *U. ohnoi MR* rate of change versus time: (**a**) 50 °C, 66 kg/m$^3$, 0.3 m/s; (**b**) 50 °C, 66 kg/m$^3$, 2.0 m/s; (**c**) 50 °C, 2 m/s, 33 kg/m$^3$; (**d**) 50 °C, 2 m/s, 100 kg/m$^3$.

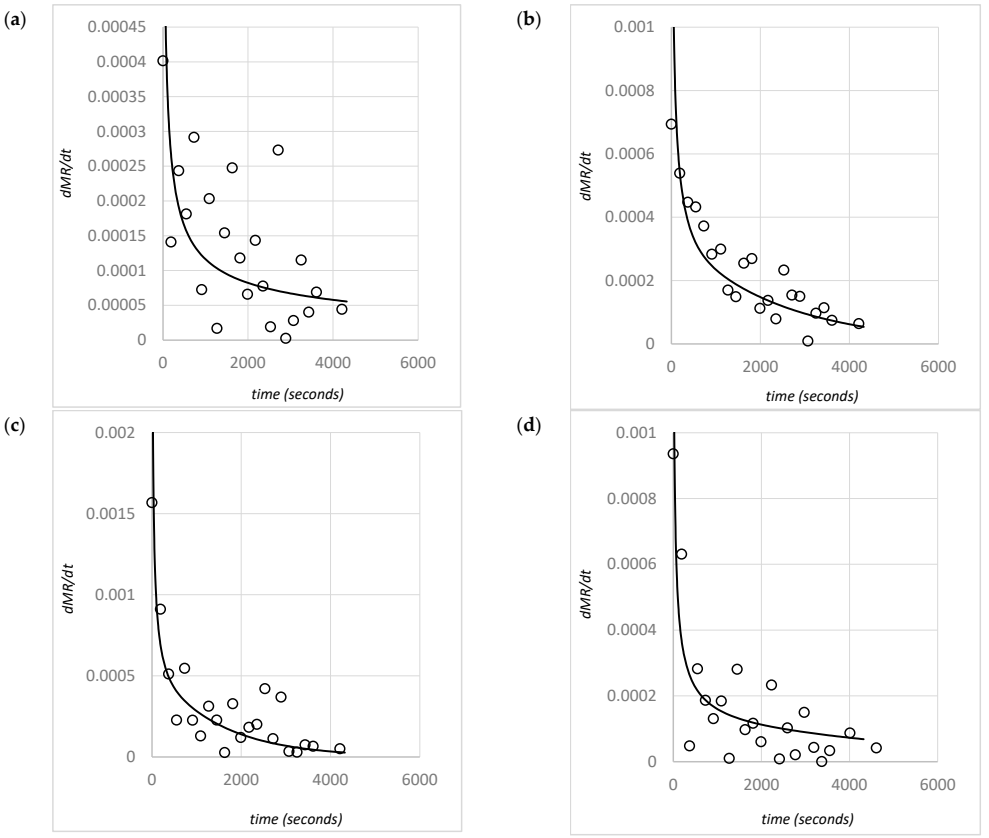


**Figure 7.** *O. intermedium MR* rate of change versus time: (**a**) 50 °C, 66 kg/m$^3$, 0.3 m/s; (**b**) 50 °C, 66 kg/m$^3$, 2.0 m/s; (**c**) 50 °C, 2 m/s, 33 kg/m$^3$; (**d**) 50 °C, 2 m/s, 100 kg/m$^3$.

### *4.2. Modeling Shrinkage*

A selection of graphs comparing the model fit between the constant $L$ (Equation (2)) and varying $L_t$ (Equation (8)) models is shown in Figures 8 and 9. In those figures, the non-shrinkage model is represented by solid lines, and the model that includes the effects of shrinkage is represented by dashed lines. In general, incorporating the effects of shrinkage into the F2L model shows a better fit to the experimental data across all conditions and both algae species. There are noticeable improvements at both the early and late stages of drying. Including shrinkage results in a lower optimized $D_e$ value. Drying is predicted to be slower initially (where the slab geometry has little change from its initial thickness) because of a lower predicted diffusivity, while it is faster during the latter stages of drying because the slab thickness is decreased. All data sets show $R^2$ values above 0.95 for *U. ohnoi*, and all but three are above 0.90 for *O. intermedium*.

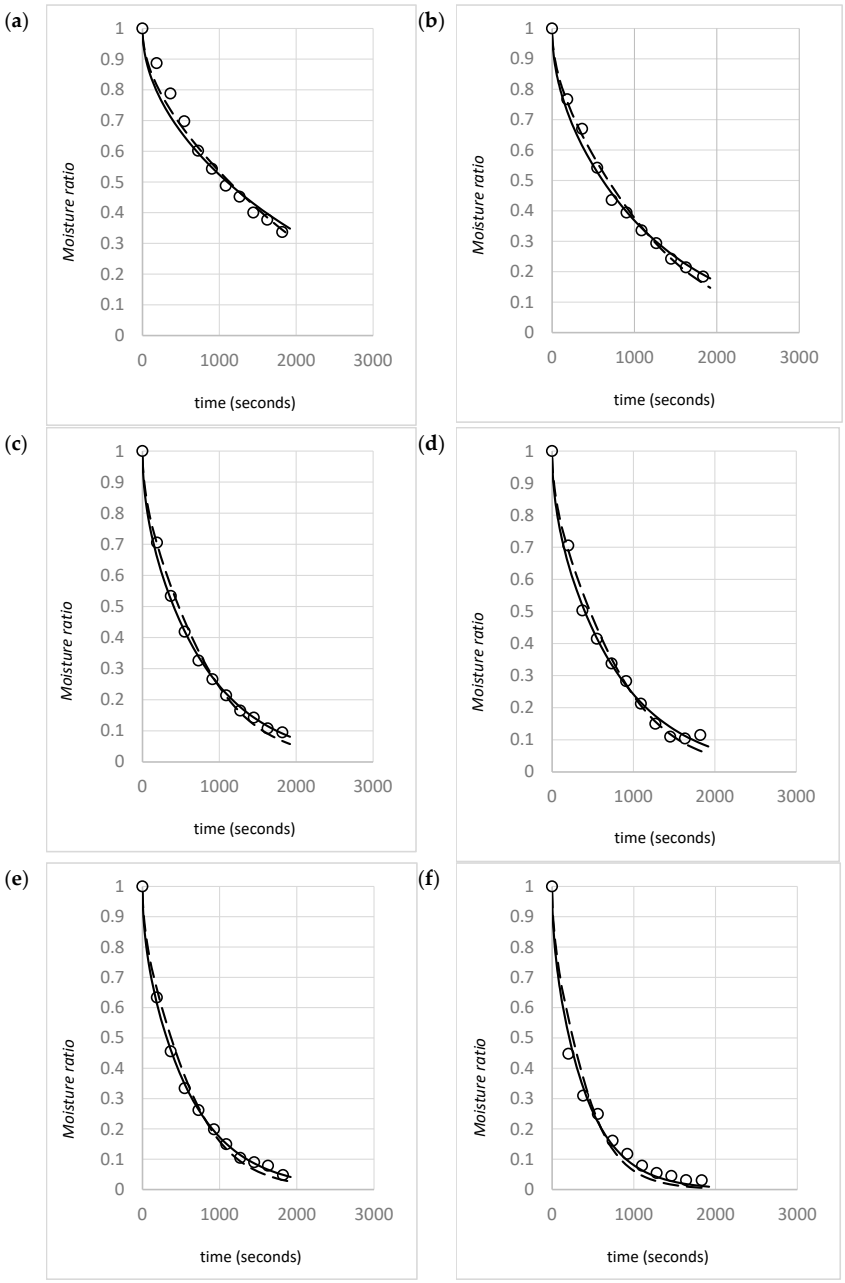


**Figure 8.** Fit comparison between constant $L$ (solid line) and $L_t$ (dashed line) models demonstrating the impact of gas velocity for *U. ohnoi* at 50 °C and 66 kg/m$^3$: (**a**) 0.4 m/s; (**b**) 0.7 m/s; (**c**) 1.1 m/s; (**d**) 1.3 m/s; (**e**) 1.7 m/s; (**f**) 2 m/s.

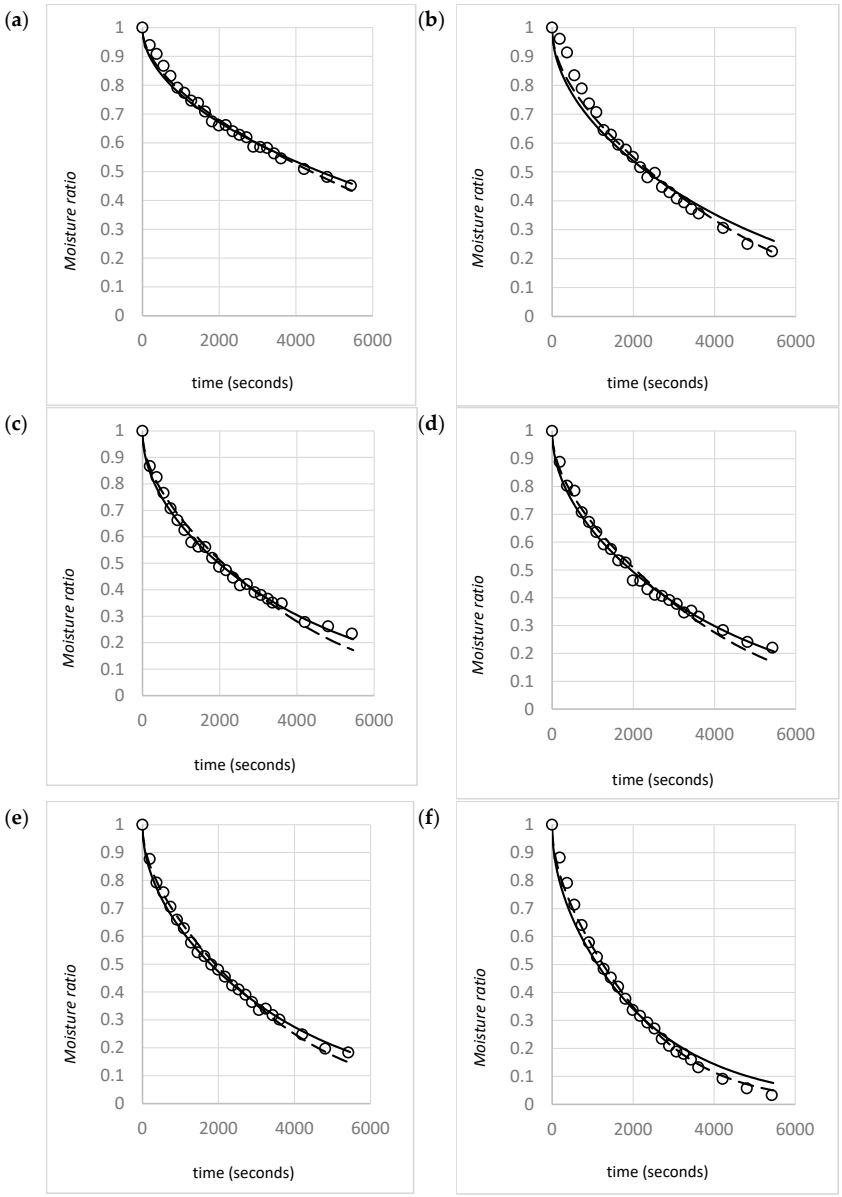


**Figure 9.** Fit comparison between constant $L$ (solid line) and $L_t$ (dashed line) models demonstrating the impact of gas velocity for *O. intermedium* at 50 °C and 66 kg/m$^3$: (**a**) 0.4 m/s; (**b**) 0.7 m/s; (**c**) 1.1 m/s; (**d**) 1.3 m/s; (**e**) 1.7 m/s; (**f**) 2 m/s.

### *4.3. Impacts of Gas Velocity and Density*

Parameter estimation for the $D_e$ values in the F2L model described in Equation (2) was used to best-fit model curves to the average of the triplicate convective drying data. The parameter-estimated values for $D_e$ and the model fit to each experimental dataset are provided in Tables 2 and 3. Figures 10 and 11 compare the model curves and experimental data (with experimental data represented by the average of triplicates) for *U. ohnoi.* Figures 12 and 13 compare model curves and experimental data for *O. intermedium*. Even without shrinkage, the general fit of the Fick's second law model to the experimental data is excellent ($R^2$ values for most experimental conditions were above 0.95). However, the model has a tendency to under-predict the experimental data for moisture ratios between 1 and 0.3, then over-predict as the moisture ratio approaches zero. As noted earlier, such issues are partially resolved by including the effects of material shrinkage, via Equation (5).

**Table 2.** $D_e$ model parameter estimation results and model fit statistics with the inclusion of volume losses for *U. ohnoi*.

| Density (kg/m$^3$) | Velocity (m/s) | $D_e$ ($10^{-8}$ m$^2$/s) | $R^2$ | RMSE | $X^2$ |
|---|---|---|---|---|---|
| 66 | 0.4 | 27.3 | 0.968 | 0.109 | 0.0047 |
| 66 | 0.7 | 45.5 | 0.989 | 0.076 | 0.0022 |
| 66 | 1.1 | 66.1 | 0.977 | 0.116 | 0.0057 |
| 66 | 1.3 | 66.7 | 0.969 | 0.139 | 0.0076 |
| 66 | 1.7 | 84.4 | 0.989 | 0.081 | 0.0027 |
| 66 | 2 | 125 | 0.971 | 0.141 | 0.0073 |
| 33 | 2 | 158 | 0.983 | 0.108 | 0.0045 |
| 50 | 2 | 151 | 0.986 | 0.101 | 0.0038 |
| 100 | 2 | 48.3 | 0.953 | 0.151 | 0.0095 |
| 33 | 0.4 | 56.1 | 0.988 | 0.085 | 0.0028 |

**Table 3.** $D_e$ model parameter estimation results and model fit statistics with the inclusion of volume losses for *O. intermedium*.

| Density (kg/m$^3$) | Velocity (m/s) | $D_e$ ($10^{-8}$ m$^2$/s) | $R^2$ | RMSE | $X^2$ |
|---|---|---|---|---|---|
| 66 | 0.4 | 6.95 | 0.957 | 0.087 | 0.0028 |
| 66 | 0.7 | 12.7 | 0.852 | 0.236 | 0.0215 |
| 66 | 1.1 | 14.7 | 0.956 | 0.119 | 0.0053 |
| 66 | 1.3 | 14.9 | 0.949 | 0.134 | 0.0068 |
| 66 | 1.7 | 16.1 | 0.856 | 0.229 | 0.0204 |
| 66 | 2 | 24.4 | 0.949 | 0.173 | 0.011 |
| 33 | 2 | 38.6 | 0.985 | 0.091 | 0.003 |
| 50 | 2 | 23.2 | 0.890 | 0.207 | 0.0175 |
| 100 | 2 | 12.2 | 0.926 | 0.139 | 0.0068 |
| 33 | 0.4 | 20.9 | 0.953 | 0.159 | 0.009 |

The results show that air velocity and material bulk density have a significant effect on the drying rate for both algae species. The drying rate increases as the air velocity increases, and the drying rate decreases as the bulk density increases, making drying fastest at high gas velocities and low bulk densities. The effect of material bulk density on the drying rate shown in Figures 11 and 13 was as expected, with increased bulk density causing a lower drying rate for both algae species. There are two mechanisms by which the bulk density affects the drying rate. The first is that increased bulk density increases the absolute amount of moisture in the material slab. More moisture being removed increases the time required to fully dry the slab of material. The F2L model cannot directly account for this change because moisture is measured as the ratio of liquid to dry solids rather than a total quantum of moisture. Because the initial moisture content described in this way does not change with bulk density, the impact of density appears as reduced effective diffusivity. In effect, an algae clump with a different density behaves as a new material and requires a new diffusion coefficient. The second mechanism is that the increased amount of material in the slab causes an increase in the physical resistance to moisture transfer (i.e., a barrier to diffusion). It makes logical sense to consider both of these effects as a part of the internal material properties that are lumped into the effective diffusivity parameter.

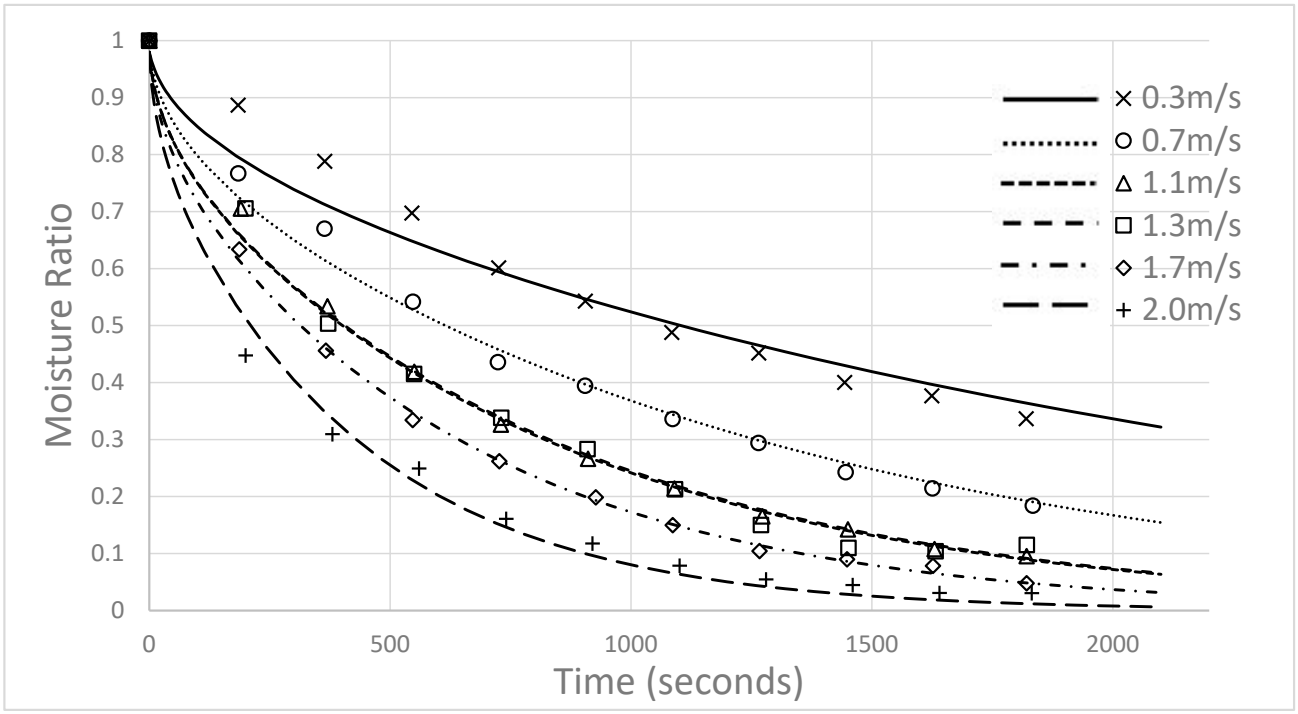


**Figure 10.** *U. ohnoi* drying model fit at varying air velocities. Temperature is 50 °C, bulk density is 66 kg/m$^3$.

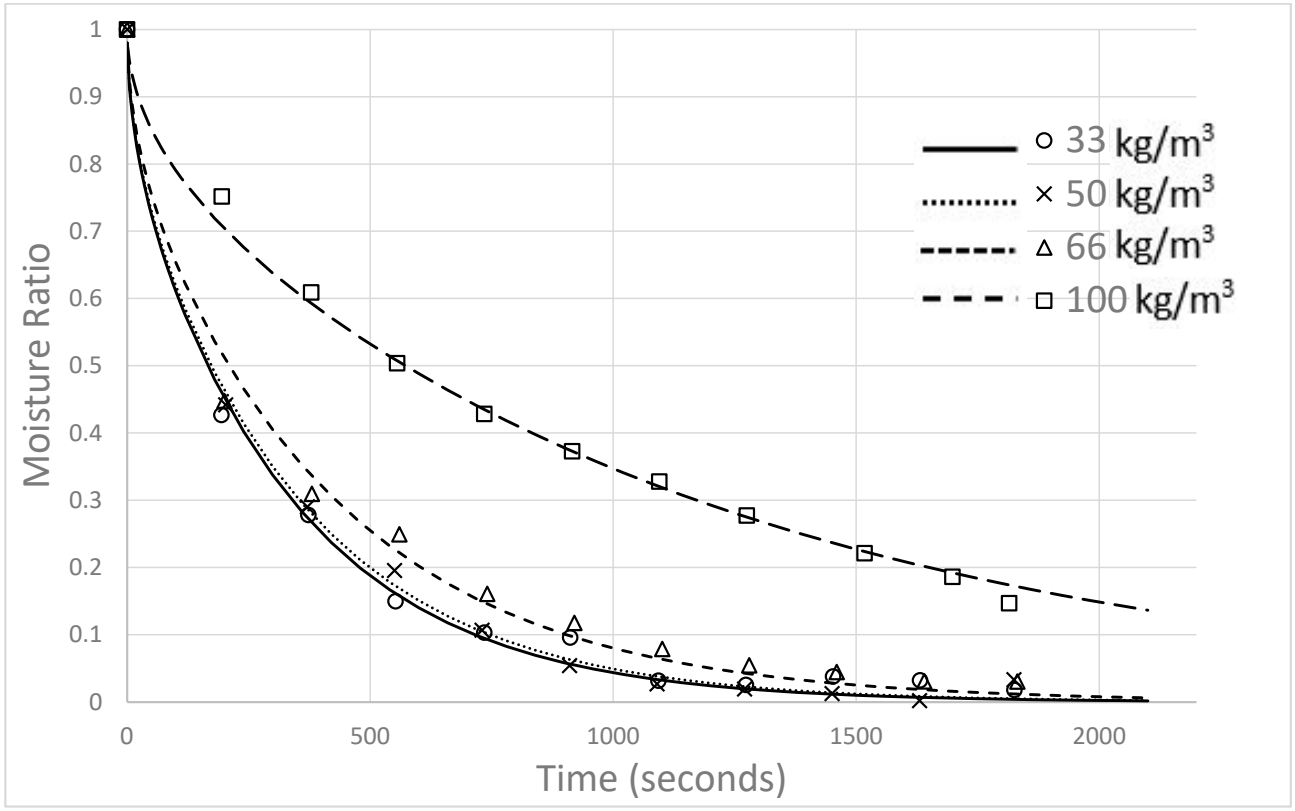


**Figure 11.** *U. ohnoi* drying model fit at varying initial bulk densities. Temperature is 50 °C, air velocity is 2 m/s.

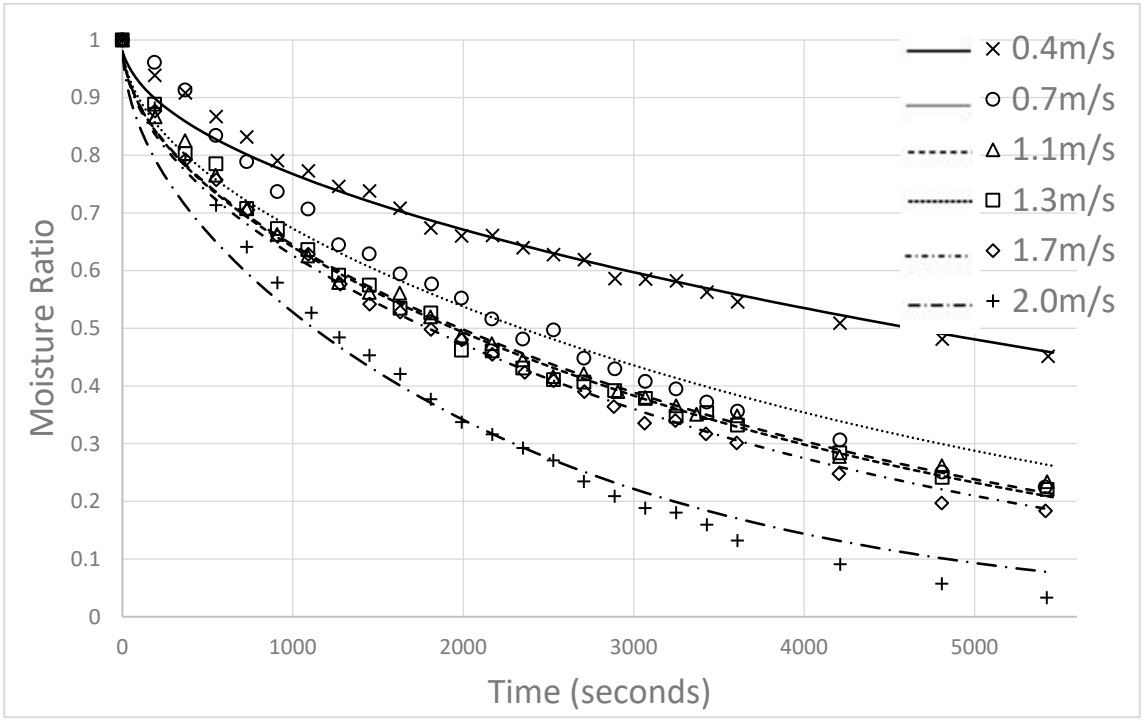


**Figure 12.** *O. intermedium* drying model fit at varying air velocities. Temperature is 50 °C, bulk density is 66 kg/m$^3$.

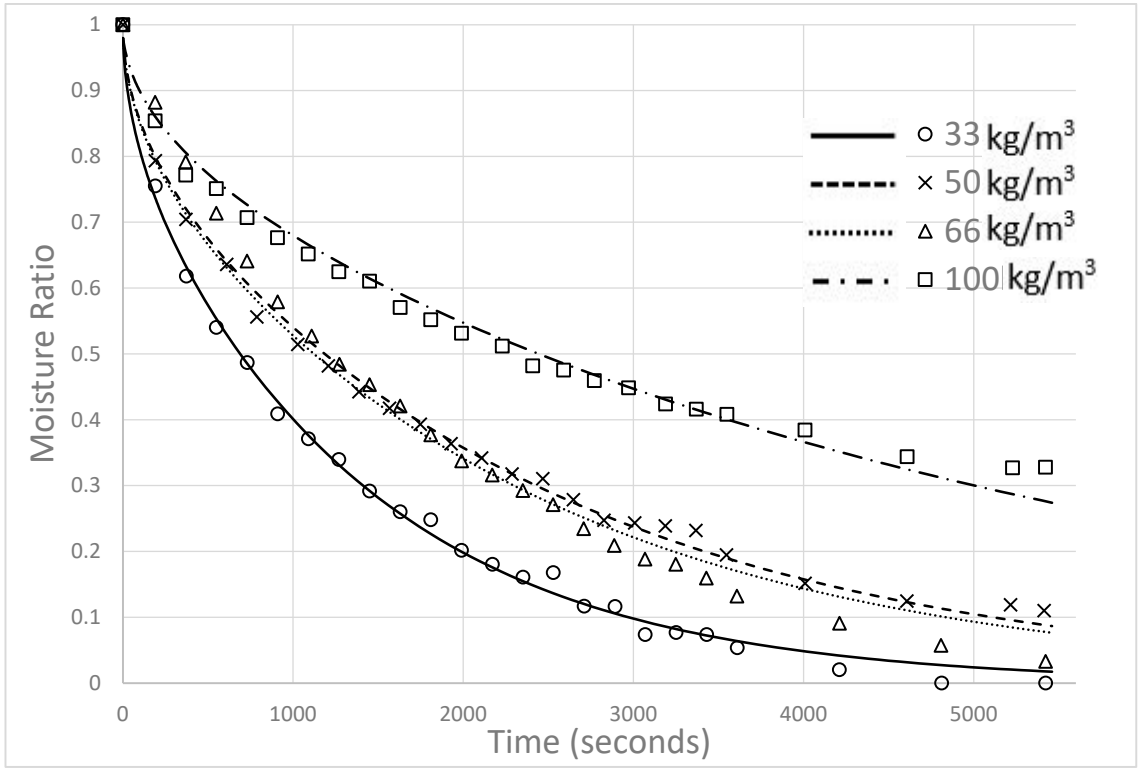


**Figure 13.** *O. intermedium* drying model fit at varying initial bulk densities. Temperature is 50 °C, air velocity is 2 m/s.

The results in Figures 10 and 12 also show that increased gas velocity causes an increased drying rate, for the conditions tested. Typically, it would be assumed that this is the result of increased convection from the material surface. However, both a Biot number

analysis (Bi > 0.1) and evidence from Figures 6 and 7 that all runs demonstrate falling-rate drying suggest that drying remains limited by internal diffusion, even as the gas velocity increases. Some studies assert the existence of a 'critical' velocity point, where further increases in gas velocity do not correspond with an increase in drying rate [32]. The results of this study did not find a critical velocity point for the range tested (0.4–2 m/s), but such a limit may exist at higher velocities. The range of velocities tested covers those typically used in industrial drying equipment. Although drying should be fastest at the critical point, an understanding of drying rates under typical equipment conditions is of significant practical value for equipment design. Gas flow rates above the range tested in this work are unlikely to be viable for use in practice.

Evidence of an Arrhenius-type relationship between effective diffusivity and temperature (Equation (3)) and the activation energies of drying ($E_a$) for both macroalgae species were determined in previous research by the authors [14]. $E_a$ is related to internal moisture binding strength (i.e., the resistance to moisture transport through a single cell) and the simplest approach is to assume that $E_a$ is a constant for a given material. Referring to Equation (3), $D_0$ varies to account for differences in the drying rate as a result of variables other than temperature (i.e., density and gas velocity). Starting with the parameter-estimated $D_e$ values obtained by fitting the F2L model described in Equation (2) to the drying data, $D_0$ values were calculated for each condition set. Statistical analysis (ANOVA) was used to determine a relationship between $D_0$, gas velocity, and initial bulk density, and to determine the significance of any interaction effects. This analysis was performed in SPSS via the general linear univariate method. The statistical analysis showed that the effect of velocity and the effect of initial bulk density were linear and significant at the 95% confidence level (with significance below 0.05). However, the interaction between velocity and initial density for both species was both much lower in magnitude and not significant at the 95% confidence level. Graphs of the trends of $D_0$ with air velocity (a) and initial density (b) are shown in Figures 14 and 15 for both species. In these figures, the thin-layer $D_0$ values taken from Walker et al., 2020 [14] are used as zero gas velocity points. These values match exceptionally well with the convective drying results and reinforce the validity of the using thin-layer experimentation to determine activation energy and diffusion coefficients for biomaterials.

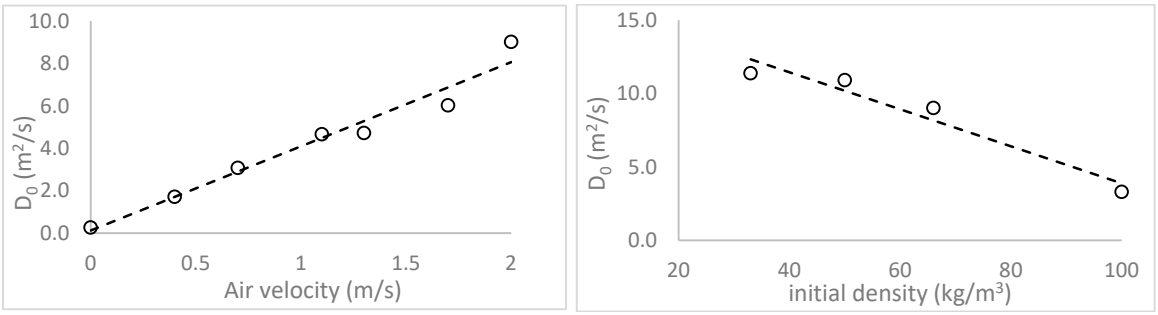


**Figure 14.** *U. ohnoi*: $D_0$ as a function of air velocity and initial bulk density.

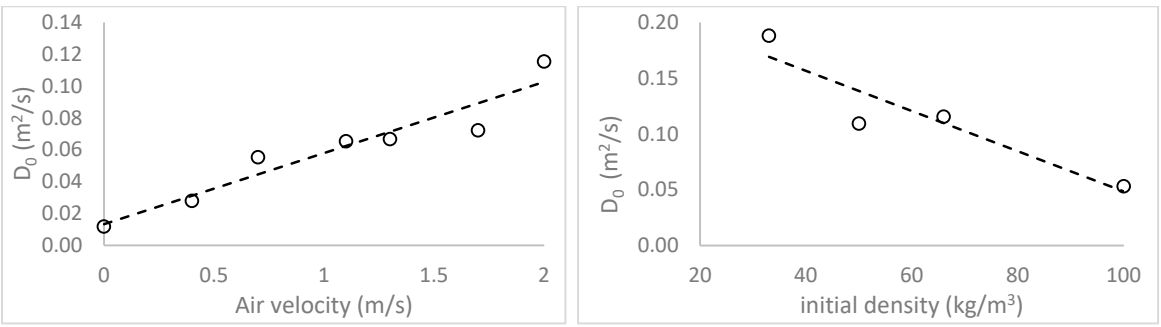


**Figure 15.** *O. intermedium*: $D_0$ as a function of air velocity and initial bulk density.

### *4.4. Diffusivity Relations*

To obtain final recommended relations for modeling macroalgae drying, the diffusivity values from parameter estimation using the shrinkage model (Equation (8)) were analyzed using SPSS. Regression models describing $D_e$ as a function of gas velocity ($v_g$) and material bulk density ($\rho$) are shown in Equation (9) (*U. ohnoi*) and Equation (10) (*O. intermedium*). The quality of the model fit to the experimental data was assessed by comparing model predictions using F2L (Equation (8)) and the effective diffusivities obtained from Equations (9) and (10) to the experimental data. Tables 4 and 5 show the statistical results of this comparison for *U. ohnoi* and *O. intermedium*, respectively.

**Table 4.** Diffusivity values calculated using Equation (9) for *U. ohnoi* and quality-of-fit parameters comparing *MR* model predictions to experimental *MR* data. All temperatures are 50 °C.

| Density (kg/m$^3$) | Velocity (m/s) | $D_e$(f($\rho$,$v_g$,$T$)) ($10^{-8}$ m$^2$/s) | $R^2$ | RMSE | $X^2$ |
|---|---|---|---|---|---|
| 66 | 0.4 | 19.4 | 0.859 | 0.230 | 0.0205 |
| 66 | 0.7 | 37.1 | 0.951 | 0.164 | 0.0102 |
| 66 | 1.1 | 60.6 | 0.971 | 0.129 | 0.0070 |
| 66 | 1.3 | 72.3 | 0.965 | 0.147 | 0.0087 |
| 66 | 1.7 | 95.9 | 0.981 | 0.111 | 0.0049 |
| 66 | 2 | 114 | 0.968 | 0.148 | 0.0081 |
| 33 | 2 | 164 | 0.983 | 0.107 | 0.0045 |
| 50 | 2 | 138 | 0.984 | 0.110 | 0.0045 |
| 100 | 2 | 61.5 | 0.894 | 0.208 | 0.0215 |
| 33 | 0.4 | 69.9 | 0.950 | 0.167 | 0.0116 |

**Table 5.** Diffusivity values calculated using Equation (9) for *O. intermedium* and quality-of-fit parameters comparing *MR* model predictions to experimental *MR* data. All temperatures are 50 °C.

| Density (kg/m$^3$) | Velocity (m/s) | $D_e$(f($\rho$,$v_g$,$T$)) ($10^{-8}$ m$^2$/s) | $R^2$ | RMSE | $X^2$ |
|---|---|---|---|---|---|
| 66 | 0.4 | 8.11 | 0.917 | 0.108 | 0.0054 |
| 66 | 0.7 | 10.8 | 0.827 | 0.236 | 0.0253 |
| 66 | 1.1 | 14.4 | 0.956 | 0.121 | 0.0054 |
| 66 | 1.3 | 16.1 | 0.941 | 0.132 | 0.0077 |
| 66 | 1.7 | 19.7 | 0.804 | 0.235 | 0.0278 |
| 66 | 2 | 22.4 | 0.943 | 0.167 | 0.0123 |
| 33 | 2 | 34.5 | 0.976 | 0.116 | 0.0047 |
| 50 | 2 | 28.2 | 0.847 | 0.233 | 0.0242 |
| 100 | 2 | 9.94 | 0.861 | 0.175 | 0.0128 |
| 33 | 0.4 | 20.2 | 0.951 | 0.159 | 0.0092 |

Model validation was undertaken on an industrial dryer processing the two algae species. The diffusivity relations described below were utilized in Equation (8) to provide *MR* versus time profiles for both species. A comparison between drying curves for both species and validation details are shown in the Supplementary Materials. The model predictions provide a reasonable match, sufficiently accurate to enable both prediction of dryer performance and dryer design. However, it should be noted that industrial dryers are subject to substantial uncertainty, and model deviation from experimental data may well be a reflection of uncertain operating conditions, material dimension assumptions, and other external factors, such as extended heating periods, rather than model accuracy. Such factors and their impact on model representativeness are more comprehensively addressed elsewhere [27].

$$U.\ ohnoi \qquad D_e = \left(4.597 + 2.79v_g - 0.0726\rho\right) \exp\left(\frac{-41,300}{RT}\right) \tag{9}$$

$$O.\ intermedium \quad D_e = \left(0.0933 + 0.029v_g - 0.00119\rho\right) \exp\left(\frac{-34,100}{RT}\right) \tag{10}$$

## 5. Discussion

The impact of material density on the drying rates of macroalgae biomaterials was as expected, with higher drying rates for less-dense clumps of algae. Only two studies were identified in the literature that examined material bulk density effects on drying rates [24,33]. Both were focused on the drying of sugar cane bagasse and showed trends similar to those observed in this research. However, the observed increases in drying rate for increasing gas velocity values are less intuitive. At first glance, such results appear to violate the fundamental assumption of a diffusion-limited system, whereby surface convection (driven by gas velocity) is assumed to *not* be the rate-limiting step. Typically, in a purely diffusion-based process, increased surface convection driven by increased gas velocity would not be expected to lead to greater rates of drying. However, several other studies have also shown a dependency between air velocity and diffusivity [22–34]. For example, Chkir et al., 2015 [23] tested effects of gas velocity on the drying kinetics and properties of brewer's grain and also showed an increase in drying rate as the gas velocity increased. Furthermore, Bezzina et al., 2018 [24] studied convective drying kinetics for sugar cane bagasse and found both diffusion-limited drying and that increased gas velocity increased the drying rate, similar to the gas velocity effects shown in this research, for macroalgae. A common theme in these results is that materials exhibiting such effects are all compressible and porous with minimum particle dimensions being smaller than bulk material dimensions.

To explain the impact of bulk material density, a mechanism involving gas penetration is proposed. Increases in material bulk density decrease the void fraction in the macroalgae slab. A decrease in void fraction results in an increase in material physically blocking the diffusion pathways to the material surface (i.e., presenting a physical resistance to diffusion) and therefore a decrease in the effective diffusivity is observed with increased density. The upper limit of this effect would be at zero void fraction, where the material can effectively be considered as a solid block, such as that represented in Figure 3, with $L$ as the full slab width. Zero void fraction would imply that there should be no opportunity for gas to penetrate into the slab, as would be expected for drying vegetable and fruit slices.

Considering the impact of gas velocity on the drying rate, experimental results in this work show that drying rates for both macroalgae increased as the drying gas velocity increased. In a porous biomaterial, it is expected that increases or decreases in air velocity cause more or less gas penetration into the particle bed, respectively. The hypothesis posed in this work is that increased penetration via a higher gas velocity works to reduce the average distance between the particle surface and the surrounding gas interaction surface (i.e., reduces the distance denoted as $L$ in Figure 3). However, in this mechanism it should be emphasized that the drying gas interaction surface is not the external edge of the material slab as defined in Figure 3, but, instead, the gas interaction surface where convection occurs is internal to the material slab due to the effect of drying gas penetration. Figure 16 illustrates this concept.

Comparing the traditional view of diffusion through a slab (Figure 3) with Figure 16, the impact of air flow can be understood by considering flow penetration acting to separate the bulk material into smaller 'blocks' of particles. Convection would then occur at the surface of these internal blocks. Thus, increases in the gas flow rate cause increased slab penetration, which breaks up the bulk material into even smaller blocks. The lower and upper limits of this mechanism are where no flow results in no penetration and $L$ is best represented as the full slab width (Figure 3). The upper limit occurs at some maximum gas velocity where the blocks are reduced to the dimensions of an individual particle or

cell width. A maximum gas velocity would reduce the geometry to that described in Figure 16b, with $L$ being equal to a single particle width. The point where this occurs could also be referred to as a 'critical' velocity in that further increases in gas flow beyond this maximum should not affect drying rates. Such a critical velocity was not observed in this work, although the existence of such a limit has been hypothesized elsewhere [32].

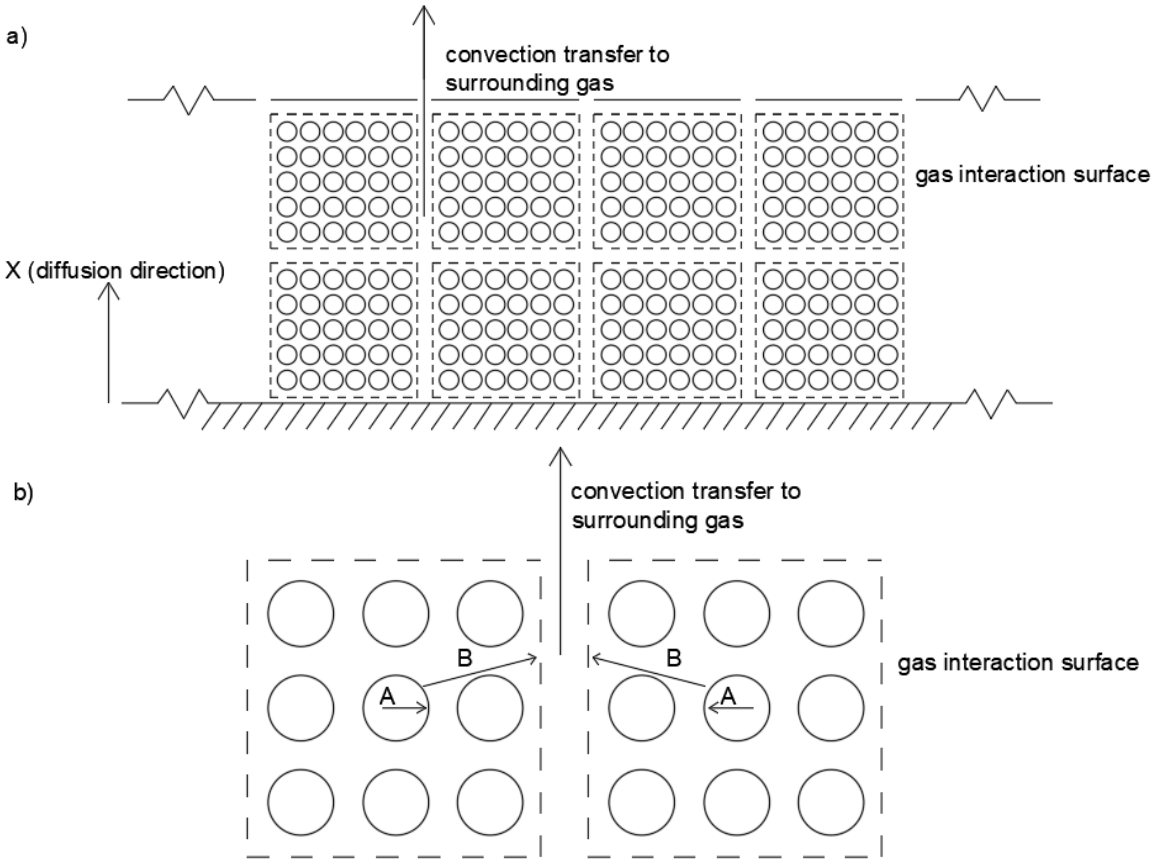


**Figure 16.** Proposed new material geometry that includes the expected mechanisms of air velocity and material density effects on drying rate. (**a**) shows the overall effect of air velocity dividing the material into smaller 'blocks' due to gas flow penetration. (**b**) shows drying mechanism and diffusive transfers within a given 'block'.

In the specific case of macroalgae where moisture is trapped within discrete cells and also within a tangled matrix of algae strands, we hypothesize that the transport process occurs via two mechanisms. Referring to Figure 16b where dotted lines represent the surfaces where convection mass transfer occurs, Mechanism A represents internal moisture diffusion through an individual cell or particle to that cell's/particle's surface, and Mechanism B represents moisture transfer through a given 'block' to the gas interaction surface. Given the incompressible nature of a single particle or cell consisting almost entirely of water, it is, instead, moisture transfer through the block (Mechanism B) that is assumed to be affected by changes in both bulk density and gas velocity. Thus, it is expected that this stage is the rate-limiting step for conditions where a relationship between air velocity and/or material bulk density and drying rates exists. Furthermore, because experimental drying data demonstrate a single falling-rate period under all experimental conditions, Mechanism B (as the rate-limiting step) is likely a diffusive transfer, supporting the use of F2L as a theoretical framework for such materials. Targeted experiments would be necessary to prove the validity of the proposed mechanism. However, it is recommended that materials with more defined dimensions and exhibiting less variability in drying rate data, such as bagasse fiber, be utilized for such work.

## 6. Conclusions

The drying rates for two species of macroalgae (*U. ohnoi* and *O. intermedium*) were determined using a convective drying apparatus under industrially relevant controlled gas flow rates (0.3–2 m/s) and controlled sample bulk densities (33–100 kg/m$^3$). Drying rates for both species were significantly impacted by both bulk density and gas velocity, and high gas velocity and low bulk density conditions provided the fastest rates of drying for both species. All drying curves demonstrated falling rate drying, indicating a diffusion-controlled drying mechanism for macroalgae drying. Fick's Second Law of diffusion, a pragmatic lumped parameter approach, and the inclusion of a model for material shrinkage enabled highly accurate predictions of moisture versus time. Accounting for shrinkage enhanced the fit of the model to the experimental data during early and late stages of drying. An excellent match between experimental drying curves and model predictions was obtained. The model was capable of accurately predicting MR versus time profiles in an industrial dryer. However, issues of scale mean that further work on adapting models to reflect larger systems is still necessary. Correlations for effective diffusivity as a function of gas velocity and material bulk density were developed. The effects of gas velocity and bulk density on drying of porous biomaterials were explained by a new mechanism for biomaterial drying that accounts for changing moisture diffusion pathways as a result of gas penetration into the bulk.

**Supplementary Materials:** The following supporting information can be downloaded at: https://www.mdpi.com/article/10.3390/cleantechnol4030041/s1, Figure S1: *U. ohnoi* pilot-scale drying. Comparison of experimental results and model predictions; Figure S2: *O. intermedium* pilot-scale drying. Comparison of experimental results and model predictions; Figure S3: Front-end view of the industrial flighted rotary dryer used for model validation; Table S1: Relevant drying conditions for each species.

**Author Contributions:** Conceptualization, C.W. and M.S.; methodology, C.W. and M.S.; software, C.W.; validation, C.W.; formal analysis, C.W.; investigation, C.W.; resources, M.S.; data curation, C.W.; writing—original draft preparation, C.W.; writing—review and editing, M.S.; supervision, M.S.; project administration, M.S. All authors have read and agreed to the published version of the manuscript.

**Funding:** This research received no external funding.

**Institutional Review Board Statement:** Not applicable.

**Informed Consent Statement:** Not applicable.

**Data Availability Statement:** Data is contained within the article or supplementary material.

**Acknowledgments:** The algal biomass used in this research was supplied by Pacific Bio Pty Ltd. as part of their research and development program on algal bioremediation and bio-products.

**Conflicts of Interest:** The authors declare no conflict of interest.

## References

1. Paris Agreement to the United Nations Framework Convention on Climate Change. Available online: https://unfccc.int/sites/default/files/resource/parisagreement_publication.pdf (accessed on 20 May 2022).
2. Sudhakar, K.; Mamat, R.; Samykano, M.; Azmi, W.; Ishak, W.; Yusaf, T. An overview of marine macroalgae as bioresource. *Renew. Sustain. Energy Rev.* **2018**, *91*, 165–179. [CrossRef]
3. Garcia-Vaquero, M.; Hayes, M. Red and green macroalgae for fish and animal feed and human functional food development. *Food Rev. Int.* **2016**, *32*, 15–45. [CrossRef]
4. Zeraatkar, A.; Ahmadzadeh, H.; Talebi, A.; Moheimani, N.; McHenry, M. Potential use of algae for heavy metal bioremediation, a critical review. *J. Environ. Manag.* **2016**, *181*, 817–831. [CrossRef]
5. Palma, H.; Killoran, E.; Sheehan, M.; Berner, F.; Heimann, K. Assessment of microalga biofilms for simultaneous remediation and biofuel generation in mine tailings water. *Bioresour. Technol.* **2017**, *234*, 327–335. [CrossRef]
6. Castine, S.; McKinnon, A.; Paul, N.; Trott, L.; de Nys, R. Wastewater treatment for land-based aquaculture: Improvements and value-adding alternatives in model systems from Australia. *Aquac. Environ. Interact.* **2013**, *4*, 285–300. [CrossRef]

7. Lawton, R.; Mata, L.; de Nys, R.; Paul, N. Algal bioremediation of waste waters from land-based aquaculture using Ulva: Selecting target species and strains. *PLoS ONE* **2013**, *8*, e0231281. [CrossRef]
8. Neveux, N.; Yuen, A.; Jazrawi, C.; Magnusson, M.; Haynes, B.; Masters, A.; Montoya, A.; Paul, N.; Maschmeyer, T.; de Nys, R. Biocrude yield and productivity from the hydrothermal liquefaction of marine and freshwater green macroalgae. *Bioresour. Technol.* **2014**, *155*, 334–341. [CrossRef]
9. Machado, L.; Kinley, R.; Magnusson, M.; de Nys, R.; Tomkins, N. The potential of macroalgae for beef production systems in Northern Australia. *J. Appl. Phycol.* **2015**, *27*, 2001–2005. [CrossRef]
10. Machado, L.; Magnusson, M.; Paul, N.; Kinley, R.; de Nys, R.; Tomkins, N. Dose-response effects of Asparagopsis taxiformis and Oedogonium sp. on in vitro fermentation and methane production. *J. Appl. Phycol.* **2016**, *28*, 1443–1452. [CrossRef]
11. Milledge, J.; Benjamin, S.; Dyer, P.; Harvey, P. Macroalgae-derived biofuel: A review of methods of energy extraction from seaweed biomass. *Energies* **2014**, *7*, 7194–7222. [CrossRef]
12. Show, K.; Lee, D.; Chang, J. Algal biomass dehydration. *Bioresour. Technol.* **2013**, *135*, 720–729.
13. Richardson, J.; Harker, J.; Backhurst, J. *Coulson and Richardson's Chemical Engineering*; Butterworth-Heinmann: Oxford, UK, 2002; Volume 2.
14. Walker, C.; Cole, A.; Antunes, E.; Sheehan, M. Equilibrium Moisture and Drying Kinetics Modelling of Macroalgae Species *Ulva ohnoi* and *Oedogonium intermedium*. *Clean Technol.* **2020**, *2*, 15. [CrossRef]
15. Hammond, L.; Bai, L.; Sheehan, M.E.; Walker, C. Experimental analysis and diffusion modelling of solar drying of macroalgae—Oedogonium sp. *Chem. Eng. Trans.* **2018**, *65*, 427–432.
16. ega-Gálvez, A.; Ayala-Aponte, A.; Notte, E.; Fuente, L.; Lemus-Mondaca, R. Mathematical modeling of mass transfer during convective dehydration of brown algae Macrocystis pyrifera. *Dry. Technol.* **2008**, *26*, 1610–1616. [CrossRef]
17. Gupta, S.; Cox, S.; Abu-Ghannam, N. Effect of different drying temperatures on the moisture and phytochemical constituents of edible Irish brown seaweed. *Food Sci. Technol.* **2011**, *44*, 1266–1272.
18. Uribe, E.; Vega-Gálvez, A.; Vásquez, V.; Lemus-Mondaca, R.; Callejas, L.; Pastén, A. Hot-air drying characteristics and energetic requirement of the edible brown seaweed Durvillaea antarctica. *J. Food Processing Preserv.* **2017**, *41*, e13313. [CrossRef]
19. Lemus, R.; Pérez, M.; Andrés, A.; Roco, T.; Tello, C.M.; Vega, A. Kinetic study of dehydration and desorption isotherms of red alga Gracilaria. *Food Sci. Technol.* **2008**, *41*, 1592–1599. [CrossRef]
20. Tello-Ireland, C.; Lemus-Mondaca, R.; Vega-Gálvez, A.; López, J.; Scala, K. Influence of hot-air temperature on drying kinetics, functional properties, colour, phycobiliproteins, antioxidant capacity, texture and agar yield of alga Gracilaria chilensis. *LWT* **2011**, *44*, 2112–2118. [CrossRef]
21. Mohamed, L.; Kane, C.; Kouhila, M.; Jamali, A.; Mahrouz, M.; Kechaou, N. Thin layer modeling of Gellidium sesquipedale solar drying process. *Energy Convers. Manag.* **2007**, *49*, 940–946. [CrossRef]
22. Djaeni, M.; Sari, D. Low temperature seaweed drying using dehumidified air. *Procedia Environ. Sci.* **2015**, *23*, 2–10. [CrossRef]
23. Chkir, I.; Balti, M.; Ayed, L.; Azzouz, S.; Kechaou, N.; Hamdi, M. Effects of air drying properties on drying kinetics and stability of cactus/brewer's grains mixture fermented with lactic acid bacteria. *Food Bioprod. Processing* **2015**, *94*, 10–19. [CrossRef]
24. Bezzina, G.; Sheehan, M.; Walker, C. The influence of gas velocity and fibre density on the drying kinetics of bagasse. In Proceedings of the 40th Annual Conference of the Australian Society of Sugar Cane Technologists, Mackay, Australia, 17–20 April 2018; pp. 424–435.
25. Chen, X.D. Moisture diffusivity in food and biological materials. *Dry. Technol.* **2007**, *25*, 1203–1213. [CrossRef]
26. Prakotmak, P.; Soponronnarit, S.; Prachayawarakorn, S. Modelling of moisture diffusion in pores of banana foam mat using a 2-D stochastic pore network: Determination of moisture diffusion coefficient during adsorption process. *J. Food Eng.* **2010**, *96*, 119–126. [CrossRef]
27. Walker, C. Modelling the Drying Kinetics of Fresh-Water and Salt-Water Macroalgae. Ph.D. Thesis, James Cook University, Townsville, Australia, 2021.
28. Montgomery, D. *Design and Analysis of Experiments*; John Wiley and Sons: Hoboken, NJ, USA, 2013.
29. Mohamed, L.; Kouhila, M.; Lahsasni, S.; Jamali, A.; Idlimam, A.; Rhazi, M.; Aghfir, M.; Mahrouz, M. Equilibrium moisture content and heat of sorption of Gelidium sesquipedale. *J. Stored Prod. Res.* **2005**, *41*, 199–209. [CrossRef]
30. Moreira, R.; Chenlo, F.; Sineiro, J.; Arufe, S.; Sexto, S. Water sorption isotherms and air drying kinetics of fucus vesiculosus brown seaweed. *J. Food Processing Preserv.* **2017**, *41*, e12997. [CrossRef]
31. Walker, C.; Cole, A.; Sheehan, M. Modelling of thin layer drying of macroalgae. In Proceedings of the 16th Asian Pacific Confederation of Chemical Congress, Melbourne, Australia, 27 September–1 October 2015.
32. Freire, F.; Figueiredo, A.; Ferrão, P. Modelling high temperature, thin layer, drying kinetics of olive bagasse. *J. Agric. Eng. Res.* **2001**, *78*, 397–406. [CrossRef]
33. Slogrove, H.; Sheehan, M.; Walker, C. Modelling and experimental determination of the drying kinetics of bagasse fibre. In Proceedings of the 39th Annual Conference of the Australian Society of Sugar Cane Technologists, Cairns, Australia, 3–5 May 2017; pp. 406–416.
34. Santacatalina, J.; Soriano, J.; Cárcel, J.; Garcia-Perez, J. Influence of air velocity and temperature on ultrasonically assisted low temperature drying of eggplant. *Food Bioprod. Processing* **2016**, *100*, 282–291.